AN ASSESSMENT OF THE DEFORMATION FIELD ASSOCIATED TO THE NOVEMBER 08, 2019 TURKMANCHAY EARTHQUAKE (MW 5.9) USING INSAR AND AFTERSHOCK DATA (NW IRAN)

Reza Saber[1]

Prof. Dr. Veysel Işık[1]

Dr. Ayşe Çağlayan[1,2]

[1]Ankara University, Department of Geological Engineering, Tectonics Research Group, Ankara, **Turkey**
[2]Ministry of Environment and Urbanization, General Directorate of Spatial Planning, Department of Geological Survey, Ankara, **Turkey**

ABSTRACT

Remote sensing studies have an essential role in identifying natural disaster risks and subsequently in urban planning. Remote sensing observations facilitate the determination of the land deformation related to active faults, saving time, and being more economical when compared with field studies. Furthermore, after earthquakes, it provides significant advantages in understanding the surface deformations and related faulting characteristics.

The arc-shaped Bozgush Mountains is a remarkable morphological feature bounded with active faults in northwest Iran. South and North Bozgush fault zones limit the southern and northern parts of this mountain belt. These active fault zones exhibit right-lateral strike slip characteristics with reverse components and have produced numerous destructive earthquakes both in historical and instrumental periods. November 8, 2019, the Turkmanchay earthquake (Mw 5.9) has occurred on the South Bozgush Fault Zone (SBFZ). As a result of this moderate earthquake, seven people died, and 529 people were injured. About 2600 buildings in 6 cities and 145 villages were damaged in different amounts, and many farm animals perished.

The absence of surface rupture during the Turkmanchay earthquake has caused discussions about the faulting characteristics which produced the earthquake. This study aims to determine and illustrate co-seismic deformation/displacement areas, which occurred after the Turkmanchay earthquake, as numerical and graphical models, by analyzing both Sentinel-1A Interferometric Synthetic Aperture Radar (InSAR) and earthquake aftershock data. Our InSAR studies have demonstrated that the deformation zone covers an area of 25×20 km^2. Results also reveal that subsidence and uplift amounts changes from -6 cm to +4 cm, respectively. The total Line Of Sight (LOS) displacement between these two maximum deformation areas is about 10 cm. Interferogram fringes and deformation patterns indicate that the direction of the potential fault that caused the earthquake is WNW-ESE. These patterns are consistent with the orientation of the SBFZ. Continuous patterns of obtained interferogram fringes indicate that the surface rupture did not occur during the earthquake. Structural discontinuities derived from the geometry of patterns coincide with the orientation of the SBFZ. Following the main earthquake, a significant number of aftershocks have occurred in the region. Observation of aftershocks in Bozgush Mountains a week after the mainshock indicates that the WNW-ESE orientation of aftershocks is consistent with the orientation of segments constituting the

SBFZ. All findings reveal that the November 08, 2019 Turkmanchay earthquake has occurred along the SBFZ.

Keywords: InSAR, Co-seismic deformation, South Bozgush Fault Zone, NW Iran

INTRODUCTION

Satellite systems provide valuable data across the entire world being wieldy used for geoscientific purposes (e.g., Abrams et al., 1988; Sabins, 1999; Saber et al., 2020; Booysen et al., 2020). Also, remote sensing data are used along with other geophysical methods in identifying all types of faults; Computer-based data processing methods of satellite images enable determining fault movements, some fault characteristics, and surface deformations triggered by active faults. InSAR (Interferometric Synthetic Aperture Radar) method is widely used and successfully applied to the geodetic technique to determine co-seismic deformations with high precision on the ground surface (e.g., Massonnet and Feigl, 1998; Bürgmann et al., 2000). Among the InSAR techniques, Differential SAR Interferometry (DInSAR) can display surface deformation in large areas with centimeter to millimeter accuracy and high spatial resolution at a relative low cost per measurement (Sansosti et al., 2010). The phase difference between the two SAR images allows to determinate the ground surface movements along the line of sight between the radar and the target within the time interval of image acquisitions (Massonnet and Feigl, 1998).

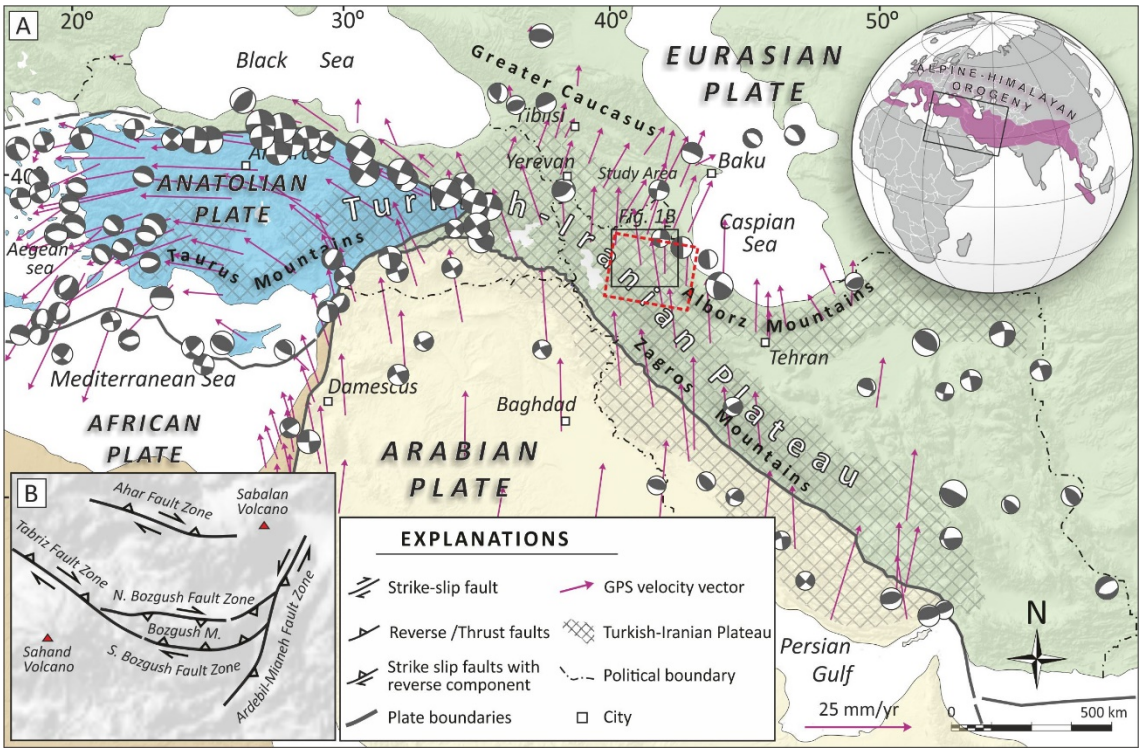

Figure 1 - A) Map showing tectonic plate boundaries within Iran and surrounding countries, the red dashed box represents the Sentinel-1A (ESA) frame from descending track 6. B) Generalized map showing main tectonic structures around Bozgush Mountains (Isik et al., 2019).

Iran is among the countries with high earthquake risk potential, due to high tectonic activities and intra-continental deformation events. These events are triggered by the collision of Arabian and Eurasian plates (e.g., Şengör and Kidd, 1979; Berberian, 1997) (Figure 1A).

NW Iran is one of the regions where earthquake events occur frequently. Active fault zones such as the Tabriz, Aras, North and South Bozgush, Ahar, Ardabil-Mianeh, Moghan, and Sangavar Fault Zones, have caused numerous destructive earthquakes in the historical time (e.g., Ambraseys and Melville, 1982; Berberian, 1997) (Figure 1B).

This study primarily focuses on determining the co-seismic deformation field of the Turkmanchay earthquake using the InSAR technique. For assessment of the deformation field associated to the November 08, 2019 Turkmanchay earthquake we analyzed synthetic aperture radar (SAR) interferograms derived from Sentinel-1A/IW data. We have used descending satellite passes to distinguish various features of the Turkmanchay earthquake, such as interferograms fringe patterns and co-seismic deformation distribution. The present study aims to reveal the fault which caused the Turkmanchay earthquake by comparing the obtained InSAR results with the field observations and earthquake aftershock data.

GEOLOGICAL OVERVIEW AND THE TURKMANCHAY EARTHQUAKE

NW Iran is a part of the Alpine-Himalayan Orogenic belt, characterized by distinct intra-continental collision and deformation processes. The arc-shaped Bozgush Mountains is one of the essential morphological structures in NW Iran, which is bounded by active/passive fault zones; some deposits of two large Neogene-Quaternary basins, called the Sarab Basin at the north and the Mianeh Basin at the south, are associated with it (Saber et al., 2018). The lithology of the Bozgush Mountains is varied and comprises Paleogene units, Mesozoic and Paleozoic units, which mostly thrusted over Neogene and Quaternary deposits. One of the important active fault zones in this region is the South Bozgush Fault Zone (SBFZ), constituting the southern boundaries of Bozgush Mountains and extending for 75 km in length and 5–10 km in width from west to the east (Isik et al., 2019). Fault segments consist of mostly right-lateral strike slip faults with a reverse component. The lateral continuities of the fault segments vary between 2 km and 13 km. General directions of these faults are NW-SE and WNW-ESE, dipping to the NE and NNE with dip angles between 45°and 76°.

On November 8, 2019, at 02:17 UTC, a 10-second earthquake of magnitude Ml:5.8/Mw:5.9 occurred near Varankesh village in Turkmanchay (East Azerbaijan, NW Iran) (International Institute of Earthquake Engineering and Seismology (IIEES), Iranian Seismological Center-IRSC) (Figure 2). The Turkmanchay earthquake originated at a relatively shallow depth of about 6-8 km and produced a strong ground shake. The epicenter location, depth, and magnitude of the earthquake seem controversial because different sources have released various parameters. USGS and IRIS have placed the epicenter of the earthquake in the northern part of the Bozgush Mountains in the Sarab Basin, whereas IIEES and GFZ have located it in the southern part of the mountains within the Mianeh Basin. Apart from these, some sources (IRSC, EMSC, BHRC) suggested that the location of the epicenter is somewhere in the central part of the Bozgush Mountains (Figure 2). Earthquake locations show uncertainties for focal depth

ranging from 6 to 19 km. Seismic records have revealed at least 225 aftershock events (until 10:00 UTC, November 09, 2019), with the largest one of magnitude 4.8 (Ml).

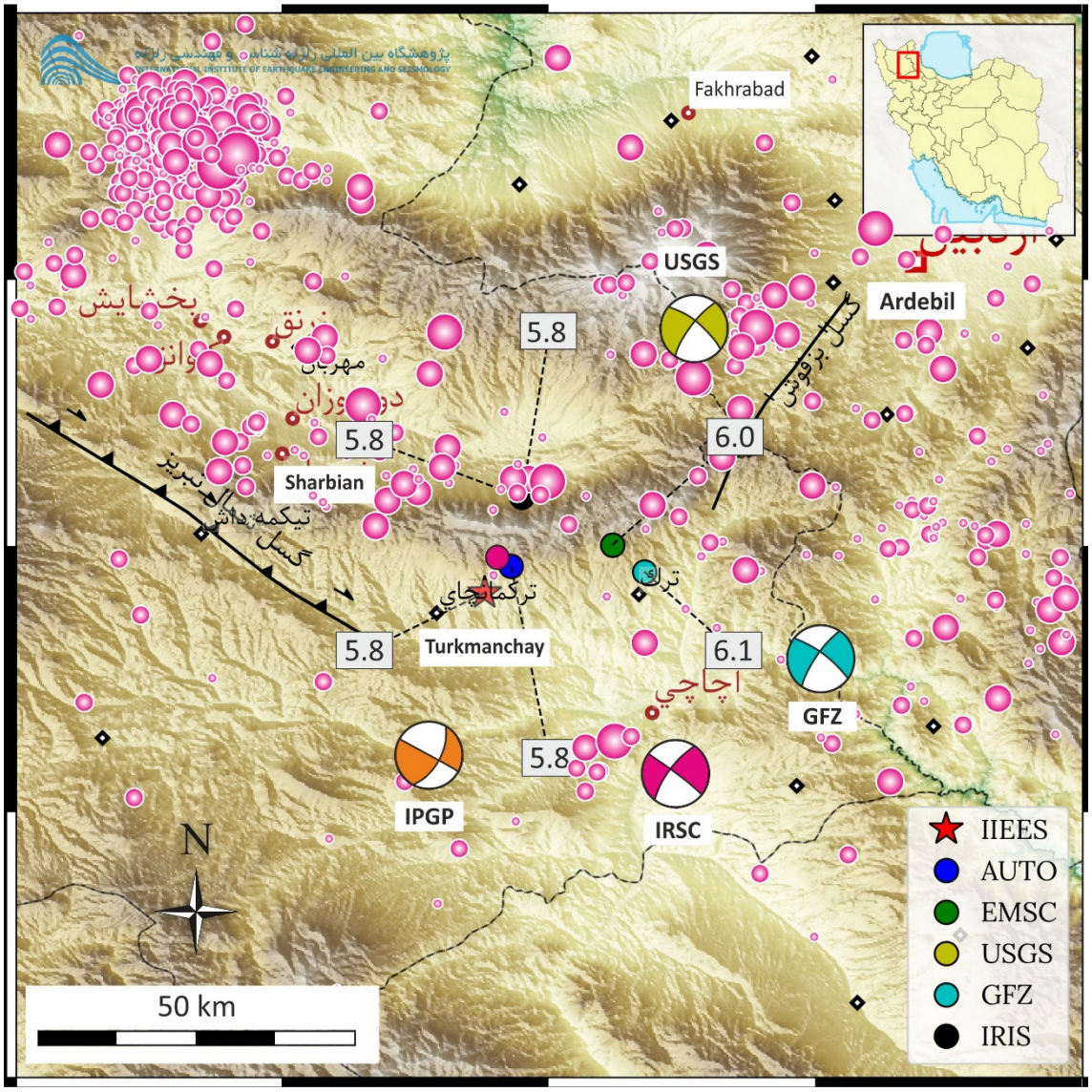

Figure 2 - Epicenter locations (IIEES) and earthquake focal mechanism solutions (EMSC and IRSC) of November 08, 2019 earthquake suggested by different institutes around the World. Purple circles indicate earthquake epicenters (1970-2019) adopted from the IRIS catalog.

METHODOLOGY

In this study, we have used two Sentinel-1A wide swath (IW) data (European Space Agency, ESA) in descending orbit, acquired on 16.10.2019 and 09.11.2019 (Figure 1A). Table 1 shows the information of two descending data used in this study. Bursts number 4 and 5 of sub-swath 2 bands of selected satellite images were used to obtain Terrain Observation with Progressive Scanning (TOPS) interferogram images (Table 1). These two bursts cover the central part of the Bozgush Mountains and surrounding areas, as well

as the Turkmanchay earthquake epicenter and related deformation area. Therefore, these two bursts were adequate to observe, measure, and interpret deformation patterns and potential displacements resulting from the November 08, 2019 Turkmanchay earthquake (Mw: 5.9). Single Look Complex (SLC) of Sentinel-1A data were processed using the Sentinel Application Platform (SNAP) software (version 7.0) provided by the European Space Agency, ENVI SARscape 5.3, and open domain algorithm SNAPHU for phase unwrapping. As a result, the Line of Sight (LOS) displacement amounts of each data pair were measured, and the terrain correction function was applied.

Table 1. The Sentinel-1A/IW data used in this study. Abbreviation: SLC-Single Look Complex

Number	Flight Direction	Observation Date	Product Type	Orbit	Track	Perpendicular Baseline (m)
1	Descending	16.10.2019	SLC	29478	6	-13
2	Descending	09.11.2019	SLC	29828	6	

INSAR RESULTS

Interferograms obtained for November 08, 2019 earthquake reflect the deformation areas formed during the earthquake with frequent and repeated fringes (Figure 3A). The presence of approximately NW-SE oriented faulting is evident where the fringes connect. The fault orientations was mapped by Isik et al. (2019). Fault kinematic analysis showed that the fault presents NE-dipping right-lateral strike slip characteristics with a reverse component. Additionally, interferogram fringes analysis indicates that numerous minor deformations and local mass movements have occurred along the main fault and the secondary fault strands (Figure 3A). The orientations of these minor discontinuities are generally parallel and sub-parallel to the direction of the main fault in the area. The large-scale mass movement during the earthquake occurred in the NW part of the main fault, possibly caused by the weakness zones associated with co-seismic deformations (Figure 3A). This mass movement covers at least 1 km^2 area in interferogram and displacement images.

LOS displacement amounts were calculated for the study from the obtained interferograms. In the obtained co-seismic deformation results for this study, the positive amounts emphasize that the LOS displacement moves toward the satellite, while negative amounts indicate the LOS displacement moves away from the satellite. LOS displacement amounts and patterns obtained from interferograms reveal characteristics and propagation of the deformation area (Figure 3B). According to descending interferogram fringes, the maximum area in which fringes are extended is about 25 km and 20 km in the N-S and E-W directions, respectively, which indicates the ellipsoidal shape of the deformation area. The highest values (positive values) were measured near the epicenter of the Turkmanchay earthquake. In this area, the maximum value (uplift) has been observed as 4 cm.

On the other hand, the highest subsidence (negative values) was observed in the southwest of the earthquake epicenter and the north-eastern part of Varankesh village. The highest subsidence values have been measured as -6 cm (Figure 3B). Accordingly, the vertical displacement between the maximum co-seismic deformation centers (positive and negative) is about 10 cm.

To understand the relationship between elevation profiles and displacement areas throughout the study area, height-displacement profiles were prepared on two different routes (Figure 3C). In the profiles, evident uplift and subsidence areas have been observed on NE and SW parts of the South Bozgush Fault Zone, respectively. Thrusting the hanging wall block of the SBFZ over its footwall is a possible reason to explain this condition.

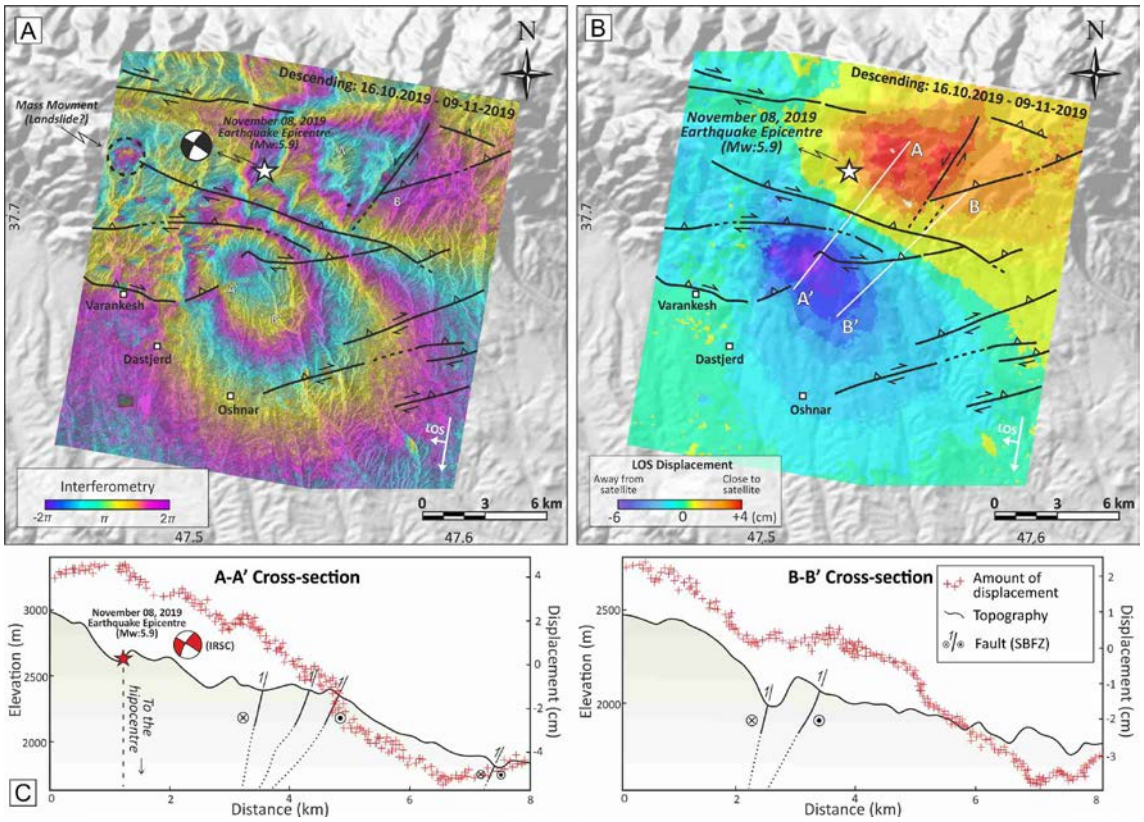

Figure 3 -A) Interferogram image for the descending orbit. The solid lines indicate major active faults (Isik et al., 2019), B) Generated displacement map of the study area, C) Elevation versus displacement cross-sections along with the profiles indicated as white solid lines in Figure B.

CONCLUSIONS

Patterns of the interferogram fringes indicate that the direction of the main fault that caused the earthquake is approximately N60°W. Field observations revealed that this 70°NE dipping fault segment has developed within the South Bozgush Fault Zone. The highest amount of deformation was observed in 7 to 10 km north-west of Varankesh village. The vertical displacement amounts vary between +4 cm (uplift) and -6 cm (subsidence) in these areas. Except for the main deformation areas related to the main fault, small scale deformation areas can also be noticed in the interferogram images and displacement model. These small scale deformation areas are related to the unstable units along slopes. The aftershocks were also tracked a week after the mainshock. Results revealed that the distribution of the aftershocks is mainly concentrated along central parts of the Bozgush Mountains from north to the south and are compatible with various fault segments. The aftershocks observed in northern parts are probably related to reactivation

of the North Bozgush Fault Zone segments, while the WNW-ESE-oriented aftershocks in central and southern parts of the Bozgush Mountains could be caused by a reactivation of different segments of the South Bozgush Fault Zone.

Acknowledgment

The authors wish to acknowledge the European Space Agency (ESA) for providing Sentinel-1 data and SNAP Software. The authors would like to thank the anonymous reviewers for their constructive comments and suggestions.

REFERENCES

Abrams M.J., Rothery D.A., Pontual A., 1988, Mapping in the Oman ophiolite using enhanced Landsat Thematic Mapper images, Tectonophysics 151, 1, pp. 387-40.

Ambraseys N.N., Melville C.P., 1982, A History of Persian Earthquakes, Cambridge University Press, New York.

Berberian M., 1997, Seismic sources of the Transcaucasian historical earthquakes. In: Historical and Prehistorical Earthquakes in the Caucasus, D Giardini and S Balassanian (eds.), NATO ASI Series 2. Environment, 28, pp. 233–311.

Booysen R., Gloaguen R. Lorenz S., Zimmermann R., Nex P.A.M., 2020, Geological Remote Sensing; In: Reference Module in Earth Systems and Environmental Sciences, (Eds.) Elias, S. et al. Elsevier.

Bürgmann R., Rosen P.A., Fielding E.J., 2000, Synthetic aperture radar interferometry to measure Earth's surface topography and its deformation, Annual Reviews of Earth Planetary Science, 28, pp. 169–209.

Isik V., Saber R., Caglayan A., 2019, South Bozqush Fault Zone: Preliminary kinematic and morphometric results, NW Iran, 38th National Geoscience Congress of Iran, Tehran.

Massonnet D., Feigl K., 1998, Radar interferometry and its application to changes in the earth's surface. Rev. Geophys., 36, 4, pp. 441–500.

Saber R., Caglayan A., Isık V., 2018, Relative tectonic activity assessment and kinematic analysis of the North Bozgush Fault Zone, NW Iran, Journal of Asian Earth Sciences, 164, pp. 219–236.

Saber R., Isik V., Caglayan A., 2020, Tectonic geomorphology of the Aras drainage basin (NW Iran): Implications for the recent activity of the Aras Fault Zone, Geological Journal, 55, pp. 5022–5048.

Sabins F.F., 1999, Remote sensing for mineral exploration, Ore Geology Reviews, 14, 3-4, pp. 157-183.

Sansosti E., Casu F., Manzo M., Lanari R., 2010, Space-borne Radar Interferometry Techniques for the Generation of Deformation Time Series: An Advanced Tool for Earth's Surface Displacement Analysis. Geophysical Research Letters, 37, 20 p.

Şengör A.M.C., Kidd W.S.F., 1979, Post-collisional tectonics of the Turkish-Iranian plateau and a comparison with Tibet, Tectonophysics, 55, pp. 361–376.